Master of Science Thesis

Optimization of ROI-based LiDAR sampling in on-road environment for autonomous driving

August 2020

Graduate School of Engineering
Seoul National University
Electrical and Computer Engineering Major

Pham Quan Dung

Optimization of ROI-based LiDAR sampling in on-road environment for autonomous driving

Supervisor: Prof. Hyuk-Jae Lee

This work is submitted as a Master of Science thesis

August 2020

Graduate School of Engineering
Seoul National University
Electrical and Computer Engineering Major

Pham Quan Dung

Confirming the master's thesis written by
Pham Quan Dung
August 2020

Chair	Prof. Cho, Nam-Ik	(Seal)
Vice Chair	Prof. Lee, Hyuk-Jae	(Seal)
Examiner	Prof. Kim, Hyun	(Seal)

본 논문작성자는 한국정부초청장학금(Global Korea Scholarship)을 지원받은 장학생임

Abstract

In recent years, light detection and ranging (LiDAR) sensors have been applied in several situations, including robotics and autonomous driving. However, LiDAR sensors have relatively low resolutions. Therefore, it is imperative to design an effective sampling algorithm for LiDAR sensors. To manage complex on-road environments, conventional ROI-based LiDAR sampling algorithm utilizes semantic information to achieve robust and high reconstruction quality. However, the ratio between sampling rates of objects, roads, and background areas is not thoroughly investigated. Therefore, the overall reconstruction quality may be degraded. To address this problem, this study presents a proposed method to examine the sampling budget ratio between objects, roads, and background areas, under the assumption that characteristics of objects, roads, and background areas are known prior to sampling. Experimental results depict a significant reduction in the mean-absolute-error (MAE) of the object region, road region and overall region by up to 45.92%, 54.18% and 3.36% under the proposed method, respectively, compared to the conventional method.

Keyword: Sampling Algorithm, Light Detection and Ranging Sensor, LiDAR, Autonomous Driving, On-road Environment, ROI-based Sampling.
Student Number: 2018-27790

Table of Contents

LIST OF FIGURE

LIST OF TABLES

Chapter 1. Introduction

1.1. Overview

Autonomous driving is a fully automated vehicle drove by itself without human supervision. [1] Should system performance degrade, the vehicle is autonomously restored to the system of minimal risk. Autonomous driving has received attention recently with the goal of reducing road accidents, congestion, and pollution; and to eliminate the huge cost of owning personal vehicles if integrated with blooming share-driving services. [2], [3] Autonomous driving, considered as the key of the future is actively developed in both academia, and industry. [4] In autonomous driving, sensors, for example cameras, GPS navigation, and light detection and ranging (LiDAR) sensors are installed in the vehicle to imitate the complex human natural sensing system. [5], [6]

Figure 1. Autonomous Driving

1.2. Light detection and ranging sensor LiDAR sampling

The LiDAR sensor is based on range sensing that estimates the time intervals between emission of light from the LiDAR and arrival of light reflected from a distant object to measure distances of objects. Therefore, within range, a LiDAR sensor can give adequate information from a wide and broad field of view (FOV). [7], [8], [9]

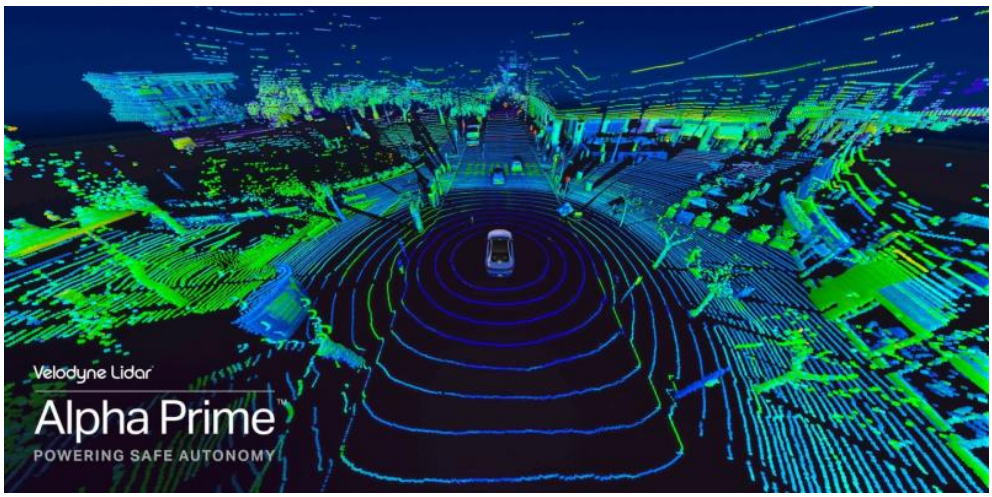

Figure 2. 3D image taken by Velodyne LiDAR

Although a LiDAR sensor detects obstacles on the road in autonomous driving, there are many challenges in utilizing this sensing in real-time applications. First, the quality of measurement from the LiDAR strongly depends on the reflective property and the angle of the reflecting surface. In practice, measurements are lost because reflected laser beams do not return during the distance measurement process. Second, despite a LiDAR sensor is able to construct a 3D map of surrounding, in order to process and store large-scale point cloud, LiDAR requires significant resources. To address these issues, fast and accurate sampling methods are proposed by Hawe et al. [10], Schwartz et al. [11], [12] and L. K. Liu et al. [13]. Nevertheless, their studies have some disadvantages.

The method by Hawe et al. [10] is not practical because prior to sampling it is required gradient of the disparity map and the difference between the gradient of color images and that of disparity maps. Schwartz et al. [11], [12] proposed a sampling method namely saliency-guided to perform sampling in a two-stage manner. For a given sampling approach, it extracts an object information or saliency from the estimated depth to select better locations. The proposed method of L. K. Liu et al. [13] is analogous to the two-stage sampling. These approaches are time-consuming rough disparity estimation. These schemes are unsuitable for autonomous driving in on-road environments owing to the complexity of background in an outdoor environment, and the reliability of gradient image of a scene in outdoor scenarios. -X. T. Nguyen et al. [14] proposed a LiDAR sampling method to distribute samples in on-road environment rely on the semantic segmentation information from regions of interest (ROI). Given a fixed sampling budgets, samples are moved from the background and road areas into an object area, significantly enhancing the quality of reconstructing objects. However, the ratio between sampling rates of objects,

roads, and background areas is not thoroughly investigated. Thus, the overall reconstruction quality may be degraded.

Chapter 2. Background

This section introduces a sampling problem and describes the ROI-based sampling algorithm, relevant sampling method to this paper.

2.1. Definition of a sampling problem

Let $x \in \mathbb{R}^N$ be an $N \times 1$ vector representing a depth map of an entire scene in a Field of View captured by LiDAR. For simplicity we assume that x is normalized so that $0 \leq x_i \leq 1$ for $i = 1, \dots, N$. Generally, it is not feasible for a LiDAR sensor acquiring data for all locations in the Field of View so that reconstructing the depth map of the entire Field of View from sampled data is necessary. A captring data is capable of acquire the number of samples M. The sampling problem is an optimization problem of selecting samples in Field of View to minimize reconstruction error with the constraint that the number of samples are the target budget M. Let $\{1, \dots, N\}$ be the set of indexes of locations of the entire Field of View and $\{i_1, \dots, i_M\}$ be the set of indexes of sampling location among $\{1, \dots, N\}$. Mathematically, we consider problem

$$\min_{i_1,\dots,i_M} \frac{1}{N} \sum_{1}^{N} \|x_j - \tilde{x}_j\| \tag{1}$$

where $x_1, \dots, x_N$ are the real values and $\tilde{x}_1, \dots, \tilde{x}_N$ are values estimated from M sampled data $x_{i_1}, \dots, x_{i_M}$

2.2. Oracle Random Sampling

2.2.1 Sampling Model

To acquire a set of spatial samples, a diagonal $S \in \mathbb{R}^{N \times N}$ is used to represent the sampling operation with the (i, j)-th entry of S being as follows

$$S_{ii} = \begin{cases} 1, & with\ probability\ p_j \\ 0, & with\ probability\ 1 - p_j \end{cases} \tag{2}$$

Where $\{p_j\}_{j=1}^{N}$ is a sequence of pre-defined probabilities satisfying $0 \leq p_i \leq 1$ and the average of probabilities must achieve a target sampling ratio ξ

$$\frac{1}{N} \sum_{j=1}^{N} p_j = \xi \tag{3}$$

Where $0 < \xi < 1$
Given S, the sample disparity map as

$$b = Sx \tag{4}$$

Based on definition of S, it is worth noting that the sampled disparity $b \in \mathbb{R}^{N\times 1}$ will contain zeros if $S_{ii} = 0$.

2.2.2 Oracle Random Scheme

Let $a = [a_1, \dots, a_N]^T$ be a vector representing the magnitude of the ground truth disparity map's gradient. It can be calculated as follows

$$a = \nabla x = \sqrt{(D_x x)^2 + \left(D_y x\right)^2} \tag{5}$$

A function of $\{a_j\}_{j=1}^{N}$ is chosen based on the intuition sampled subset of gradient should carry the maximum of amount of information compared to the full set of gradients. To capture this intuition, it is to require that the average gradient computed from all N samples is identical to average gradient computed from subset of ξN samples. The average gradient computed from all samples is as follows

$$\mu \stackrel{\text{def}}{=} \frac{1}{N}\sum_{j=1}^{N} a_j \tag{6}$$

The average gradient computed from a random subset of ξN samples is as follows

$$Y \stackrel{\text{def}}{=} \frac{1}{N}\sum_{j=1}^{N} \frac{a_j}{p_j} I_j \tag{7}$$

Where $\{I_j\}_{j=1}^{N}$ is a sequence of Bernoulli random variables with probabilities $\Pr[I_j = 1] = p_j$. Here, the division of a_j by p_j is to ensure that Y is biased, i.e, $\mathbb{E}[Y] = \mu$.

Minimizing the difference between Y and μ can be achieved by minimizing the variance $\mathbb{E}[(Y-\mu)^2]$

$$\mathbb{E}[(Y-\mu)^2] = \frac{1}{N}\sum_{j=1}^{N} \frac{{a_j}^2}{{p_j}^2} Var[I_j] \tag{8}$$

Since $Var[I_j] = p_j(1-p_j)$. Variance $\mathbb{E}[(Y-\mu)^2]$ is as follows:

$$\mathbb{E}[(Y-\mu)^2] = \frac{1}{N}\sum_{j=1}^{N} {a_j}^2 \left(\frac{1-p_j}{p_j}\right) = \frac{1}{N}\sum_{j=1}^{N} \left(\frac{{a_j}^2}{p_j} - {a_j}^2\right) \tag{9}$$

It can be seen that the optimal sampling probabilities $\{p_j\}_{j=1}^{N}$ can be obtained by solving the optimization problem

$$\min_{p_1,\dots,p_N} \frac{1}{N}\sum_{j=1}^{N} \frac{{a_j}^2}{p_j} \tag{10}$$

subject to $\frac{1}{N}\sum_{j=1}^{N} p_j = \xi \ , \ 0 \le p_j \le 1$

The solution is formulated as follows

$$p_j = \min(\tau a_j, 1) \tag{11}$$

Where τ is the solution of $g(\tau) = 0$. Here,

$$g(\tau) = \sum_{j}^{N} \min(\tau a_j, 1) - \xi N \tag{12}$$

2.3. ROI-based LiDAR sampling algorithm

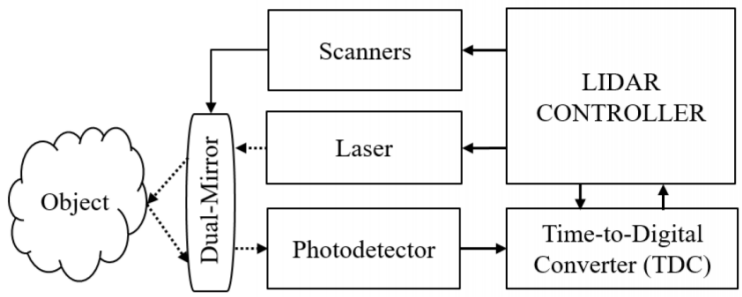

Figure 3. LiDAR diagram [9], [14]

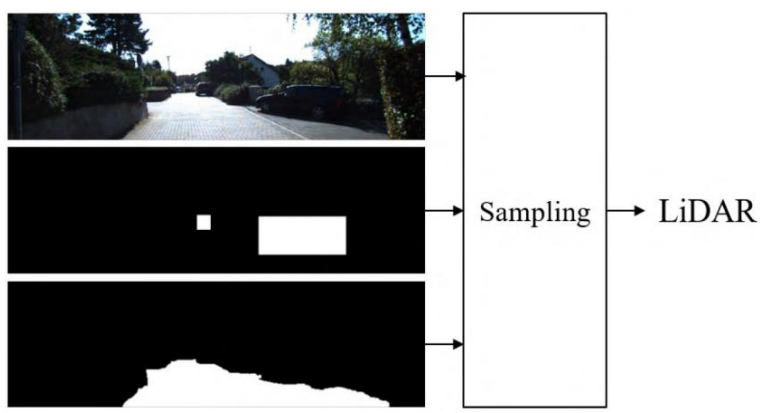

Figure 4. LiDAR ROI-based sampling system configuration [9], [14].

There are two main reasons make previous sampling schemes inappropriate to apply for autonomous driving in on-road environment. Firstly, in general, a scene in an outdoor environment composes of complex background; this engendered previous approaches to allocate excessively high number of samples into non-interested areas. Secondly, obtaining a reliable gradient image of a scene in an outdoor environment, generally, is a challenging task owing to the complication of its RGB image and the sparseness of its raw depth image to estimate a reliable gradient. To tackle the sampling problem in an on-road environment, it is assumed to apply the state-of-the-art road and object detection algorithms to segment a scene into three regions namely

road, object, and background.

Let S_o, S_R, and S_B be the index sets of points in object, road, and background regions, respectively. The union of the three sets is the set of sample budget, and the intersection of any two is an empty set.

$$S_o \cup S_R \cup S_B = \{1, 2, \dots, N\} \tag{13}$$

$$S_o \cap S_R = \ S_o \cap S_B = S_B \cap S_R = \emptyset \tag{14}$$

Object, road and background regions have different characteristics so that it is likely to sample them with different priorities. Let λ_O, λ_R and λ_B be weighted-parameters denoting sampling priorities for the object, road and background areas, respectively. A road area is generally flat so that the MAE does not change dramatically when the sampling rate changes. As a result, the parameter λ_R for a road area is less than the one for a background area. λ_B, λ_O and λ_R must satisfy the equations as follows:

$$\lambda_O = \alpha\lambda_B \tag{15}$$

$$\lambda_R = \beta\lambda_B \tag{16}$$

For a given sampling ratio ξ, the prior map, and parameters α and β, the derivation of the optimal sampling probability $\{p_j\}_{j=1}^{N}$ is formulated as the following optimization problem:

$$\min_{p_1,\dots,p_N} \frac{1}{N}\left(\sum_{i\in S_B}\frac{a_i^2}{p_i} + \alpha\sum_{j\in S_O}\frac{a_j^2}{p_j} + \beta\sum_{k\in S_R}\frac{a_k^2}{p_k}\right) \tag{17}$$

$$\text{subject to } \frac{1}{N}\sum_{j=1}^{N} p_j = \xi \ , \ 0 \le p_j \le 1$$

Obviously, given weight parameters α and β are derived by solving the optimization as follows:

$$\min_{\alpha,\beta} \frac{1}{N}\left(MAE_{obj} + \lambda MAE_{all}\right) \tag{18}$$

Chapter 3. Proposed method

This research proposes methods to distribute samples efficiently in road and object regions to enhance the reconstruction quality of object and road areas, and overall area.

3.1. Analytical method

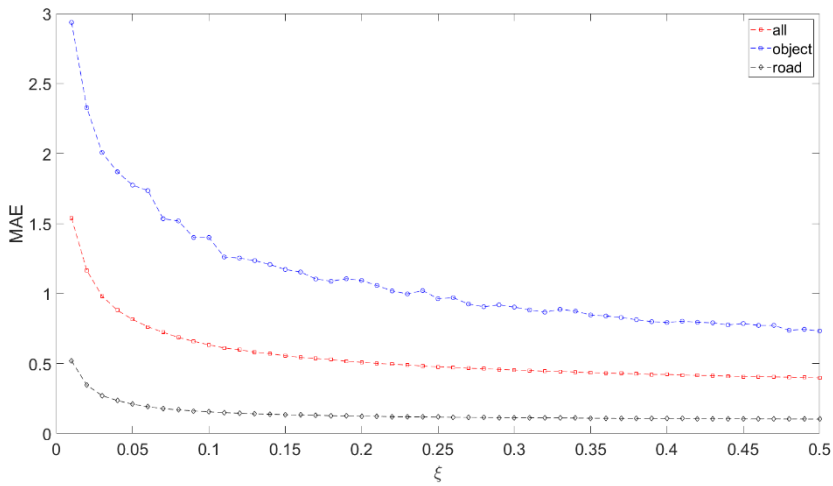

Figure 5. Average mean absolute error over sampling rates

Given a target sampling ratio ξ, the problem is to distribute the sampling ratio for specific region as object, road and background in order to minimize the reconstruction error in object, road, background region or overall image. The reconstruction error is solely capable of being calculated after sampling. Therefore, it is assumed that MAE has to be predicted prior sampling so as to optimize final output. Fig. 1 illustrates the MAEs of object, road areas and background scenes for specified sampling rates from 1% to 50%. By examining on various images, it is evident that the these MAEs can be modeled as functions $f_O(x)$, $f_R(x)$, $f_B(x)$ such that $f_O: [0,1] \mapsto \mathbb{R}_+$, $f_R: [0,1] \mapsto \mathbb{R}_+$, $f_B: [0,1] \mapsto \mathbb{R}_+$. It is noticeable that although graphs are similar in case of MAE of all, MAE of object and MAE of road, which are shown in Fig. 4 and Fig. 5, the parameters a_O, b_O, c_O, a_R, b_R, c_R, a_B, b_B, c_B vary depending on the area of object and road.

$$MAE_{obj} = f_O(\lambda_O) = a_O + \frac{b_O}{c_O + \lambda_O} \tag{19}$$

$$MAE_{road} = f_R(\lambda_R) = a_R + \frac{b_R}{c_R + \lambda_R} \tag{20}$$

$$MAE_{background} = f_B(\lambda_B) = a_B + \frac{b_B}{c_B + \lambda_B} \tag{21}$$

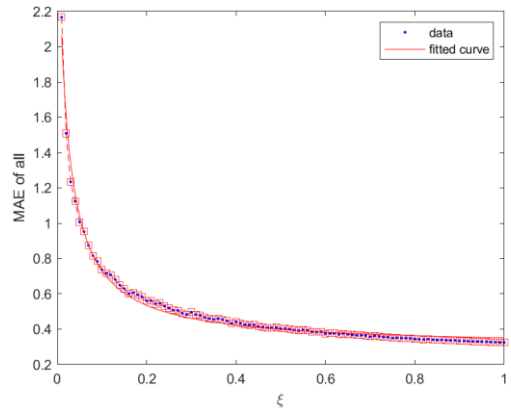

(a)

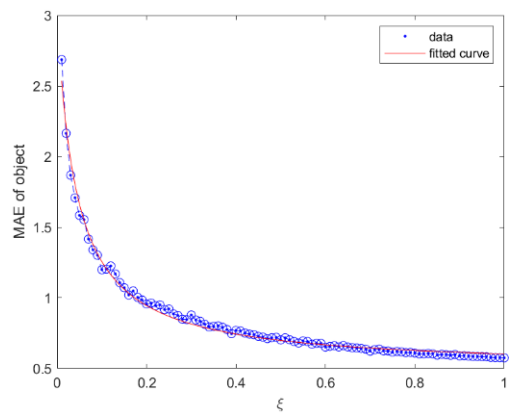

(b)

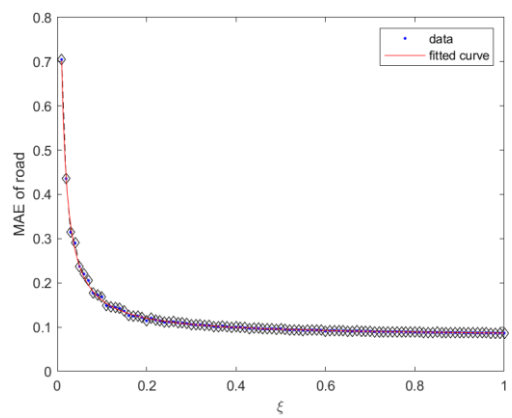

(c)

Figure 6. MAE of overall, object and road areas in case $\Delta S_O < \Delta S_R$, (a) Overall area, (c) Object area, and (c) Road area.

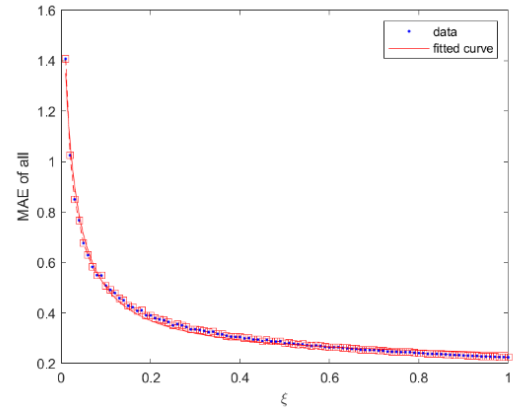

(a)

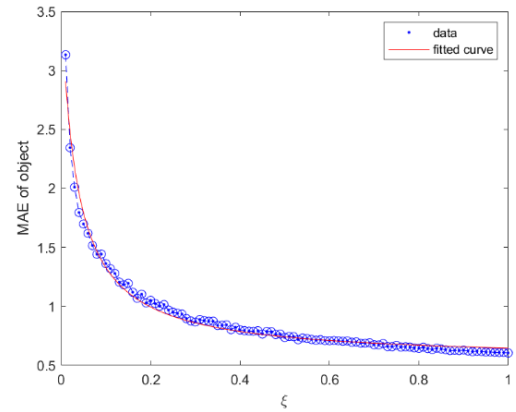

(b)

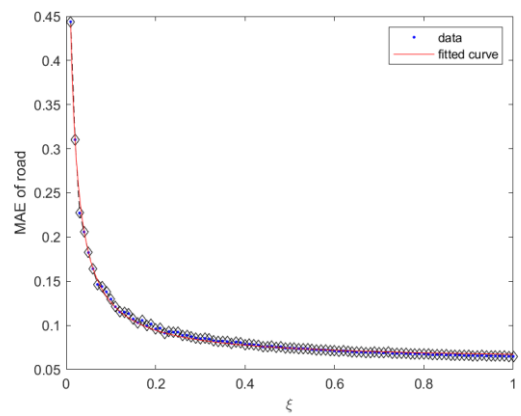

(c)

Figure 7. MAE of overall, object and road areas in case $\Delta S_O > \Delta S_R$, (a) Overall area, (c) Object area, and (c) Road area

For consistency, let $a = [a_1, \dots, a_N]^T$ be a vector indicating a prior information of a depth map. For a given sampling ratio ξ, the prior map, and parameters α and β, respectively, the derivation of the optimal sampling probability $\{p_j\}_{j=1}^{N}$ is formulated as the following optimization problem

$$\min_{p_1,\dots,p_N} \frac{1}{N}\left(\phi_B \sum_{i\in S_B} \frac{a_i^2}{p_i} + \phi_O \sum_{j\in S_O} \frac{a_j^2}{p_j} + \phi_R \sum_{k\in S_R} \frac{a_k^2}{p_k} \right) \tag{22}$$

Subject to

$$\frac{1}{N}\left(\sum_{i\in S_B} p_i + \sum_{j\in S_O} p_j + \sum_{k\in S_R} p_k \right) = \xi \tag{23a}$$

$$\frac{1}{|S_R|}\sum_{k\in S_R} p_k = \beta \quad \frac{1}{|S_B|}\sum_{i\in S_B} p_i \tag{23b}$$

$$\frac{1}{|S_O|}\sum_{j\in S_O} p_j = \alpha \quad \frac{1}{|S_B|}\sum_{i\in S_B} p_i \tag{23c}$$

Where ϕ_B, ϕ_O, ϕ_R are the weights for background, object, and road, respectively. ϕ_B, ϕ_O, ϕ_R are chosen based on which area is more important in optimization. Overall, $\phi_B = \phi_O = \phi_R = 1$ shows a better performance in overall reconstruction.

In this model, it is pivotal to note that it is assumed (19), (20) and (21) are determined prior sampling, which means that the parameters a_O, b_O, c_O, a_R, b_R, c_R, a_B, b_B, c_B are known prior sampling. From characteristics of object, road and background, it is obvious that the background and object areas are not flat. Therefore, to minimize the total errors of object, road, and background, this optimization problem can be expressed as follows:

$$\min_{\alpha,\beta,\lambda_B} \left(\phi_B MAE_{background} + \phi_O MAE_{obj} + \phi_R MAE_{road} \right) \tag{24}$$

Because the total sampling budget of whole image must be maintained, the following constraint holds:

$$\lambda_O S_O + \lambda_R S_R + \lambda_B S_B = \xi \tag{25}$$

Where

$$\lambda_O = \alpha\lambda_B, \ \lambda_R = \beta\lambda_B \tag{26}$$

And ξ, λ_O, S_O, S_R and S_B are the sampling ratios of whole image, object area, road area, and background area, the ratio of object area to whole image, the ratio of road area to whole image, the ratio of background area to whole image, respectively.

From (25), and (26), it can be deduced that:

$$\beta = -\frac{S_O}{S_R}\alpha + \frac{\xi}{\lambda_B S_R} - \frac{S_B}{S_R} \quad (27)$$

From (25), (26), and (27):

- For $\alpha \geq 0$:

$$\xi - \lambda_B S_B \geq 0 \quad (28)$$

- For $\beta \geq 0$:

$$\xi - \lambda_B S_B - \alpha\lambda_B S_O \geq 0 \quad (29)$$

The optimization problem in (24) can be solved with constraints in (25), (26). (28) and (29). The optimal solutions are as follows

$$\lambda_b = \frac{c_r + \frac{\xi}{S_r} + \frac{S_o}{S_r}c_o - \left(\frac{S_o}{S_r}\sqrt{\frac{\phi_O b_o S_b}{\phi_B b_b S_o}} + \sqrt{\frac{\phi_R b_r S_b}{\phi_B b_b S_r}}\right)c_b}{\sqrt{\frac{\phi_R b_r S_b}{\phi_B b_b S_r}} + \frac{S_b}{S_r} + \frac{S_o}{S_r}\sqrt{\frac{\phi_O b_o S_b}{\phi_B b_b S_o}}} \quad (30)$$

$$\alpha = \sqrt{\frac{\phi_O b_o S_b}{\phi_B b_b S_o}} + \frac{c_b\sqrt{\frac{\phi_O b_o S_b}{\phi_B b_b S_o}} - c_o}{\lambda_b} \quad (31)$$

Figure 6, 7, 8, 9 show the objective function (24) and the result to solve optimization problem of this objective function. Variations of this objective function can be found in the Appendix section.

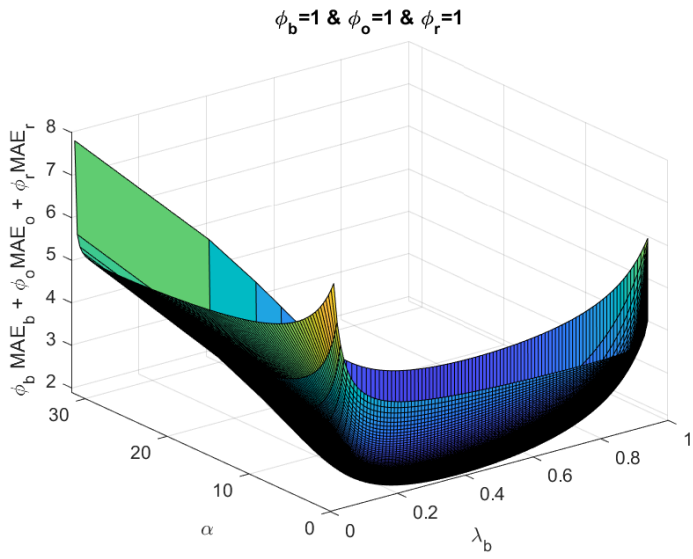

Figure 8. Graph of objective function

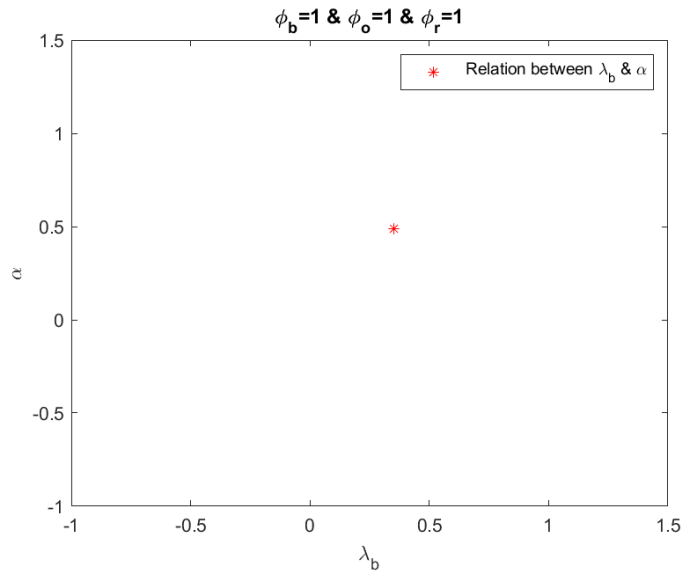

Figure 9. Relation between λ_b and α

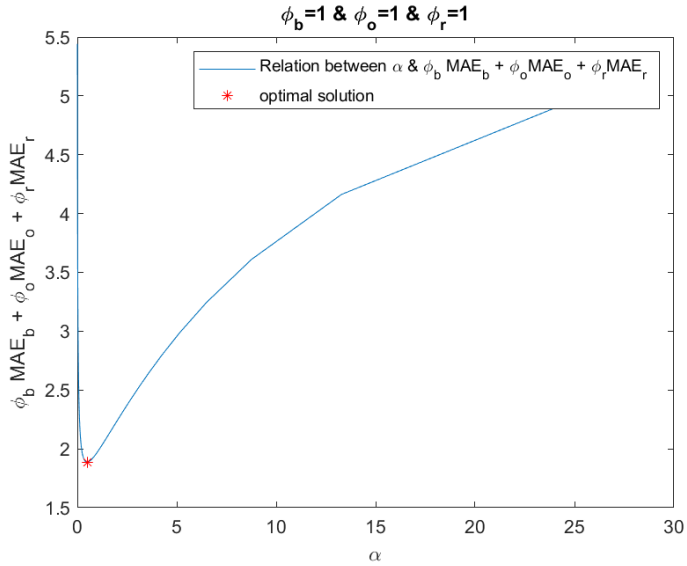

Figure 10. Relation between α and $\Phi_b MAE_b + \Phi_o MAE_o + \Phi_r MAEr$

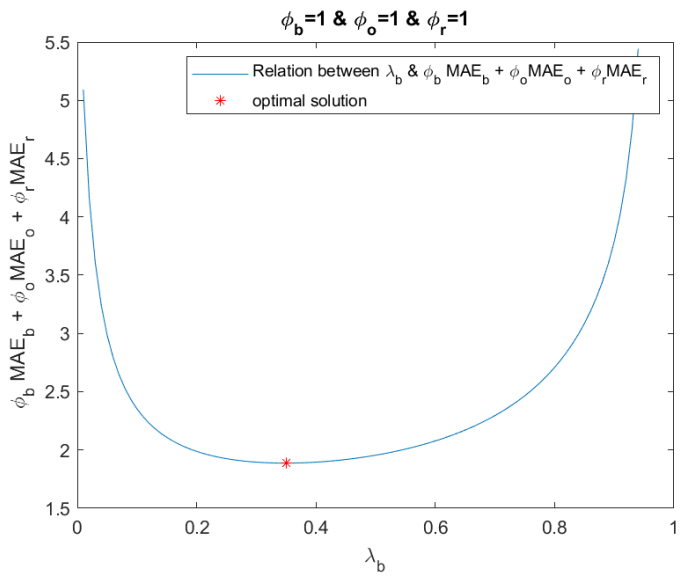

Figure 11. Relation between λ_b and $\Phi_b MAE_b + \Phi_o MAE_o + \Phi_r MAEr$

Chapter 4. Experimental results

4.1. Dataset

This section evaluates the proposed method on KITTI datasets [5]. KITTI dataset consists of camera images, laser scans, high-precision GPS measurements, and IMU accelerations from a combined GPS/IMU system. Depth images are used in evaluation. They are acquired by projecting point cloud data into a color image domain. The raw depth map, which is taken by using Velodyne HDE64 sensor [8], is used as the input and ground truth is used for evaluation. It is known that the combination of 11 raw scans creates the ground truth image.

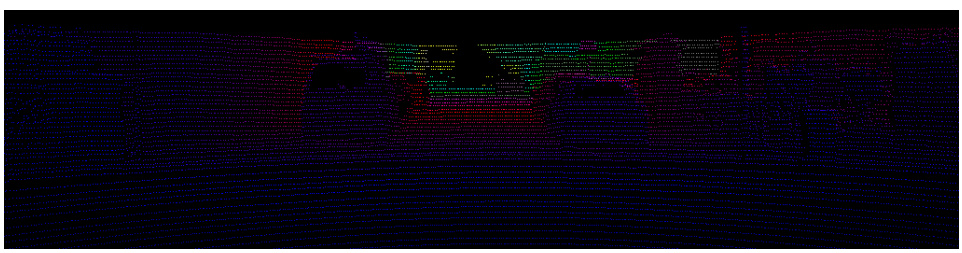

Figure 12. Raw scan from KITTI

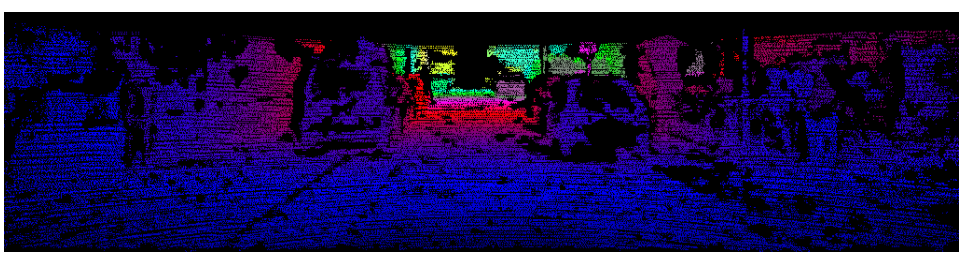

Figure 13. Ground truth depth from KITTI

Figure 14. RGB image of scene

4.2 Quantitative evaluation

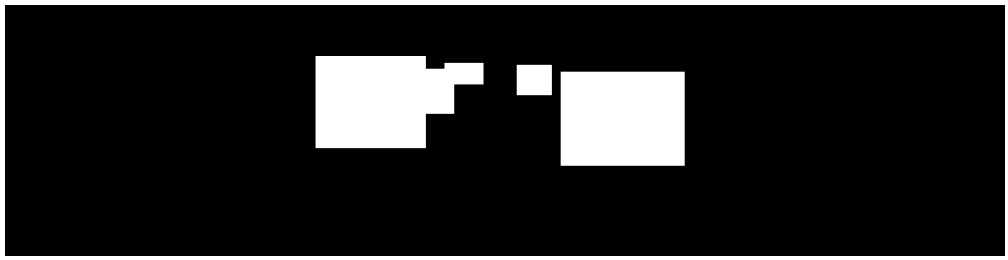

Figure 15. Object segmentation

Figure 16. Road segmentation

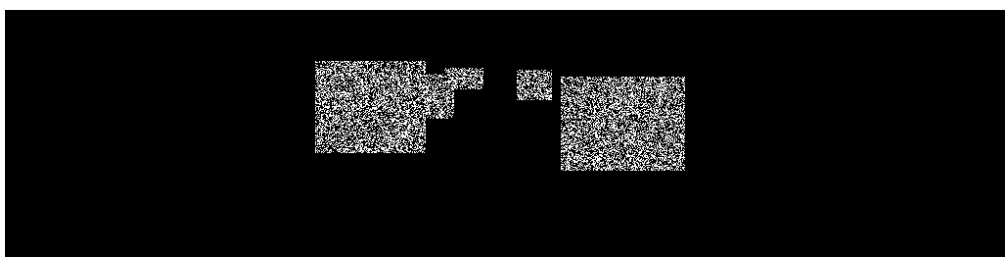

Figure 17. Sample on object area

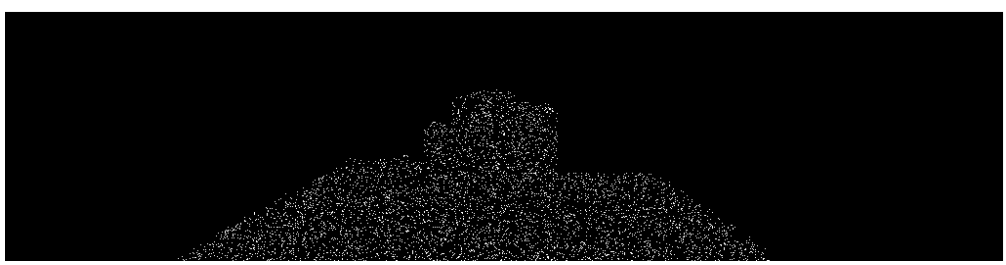

Figure 18. Sample on road area

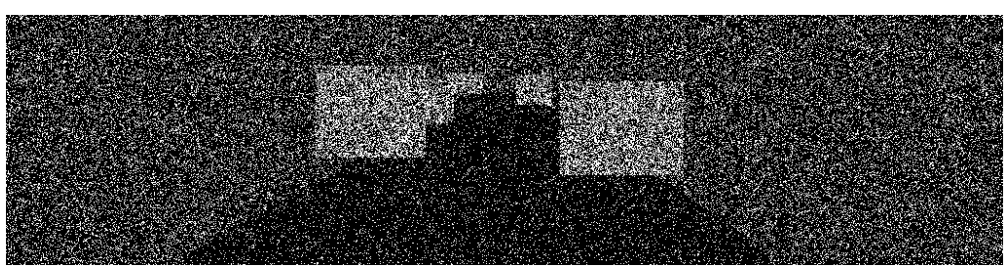

Figure 19. Sample on image

This section compares the performance of the proposed method with existing method ROI-based LiDAR sampling algorithm. This study attempts to optimize the previous research of ROI-based LiDAR sampling algorithm in on-road environment. According to –X.T.Nguyen et al. [14], the research proposed a scheme detects the object areas. From the segmentation results, the approach distributes samples across the segmented areas. However, the ratio between sampling rates of object, road and background regions is not fully investigated. In our study, the ratio sampling rates is introduced in order to achieve better performance.
The comparison of the MAEs on object, road, background and overall areas are shown in TABLES 1, 2, 3, and 4, respectively. On each table, the first, second, and third rows shows the results with three variations of ROI-based sampling algorithm and the fourth, fifth, sixth, seventh, eighth, ninth display the proposed method with different with different weight for object, road and background. In each row, the second, third, fourth, and fifth columns represent the results with the sampling rates of 5%, 10%, 15%, and 20%, respectively.

As can be seen in TABLE 1, the MAEs of object areas using proposed method are fairly low, in case of sampling rate 5% and 10%, it worth noting that MAEs of object area considerably decrease when applying proposed method by up to 43.83%. Data in TABLE 1 suggest that proposed method is suitable for low sampling rate. Objects represent for cars, trucks, or pedestrians.

	5%	10%	15%	20%
ROI-based sampling ($\alpha = 1, \beta = 1$)	1.372	1.289	1.097	1.065
ROI-based sampling ($\alpha = 4, \beta = 1$)	1.166	0.909	0.724	0.701
ROI-based sampling ($\alpha = 4, \beta = 0.25$)	0.727	0.637	0.610	0.639
Proposed method ($\emptyset_O = 1, \emptyset_R = 1, \emptyset_B = 1$)	0.893	0.760	0.702	0.668
Proposed method ($\emptyset_O = 2, \emptyset_R = 1, \emptyset_B = 1$)	0.697	0.626	0.595	0.581
Proposed method ($\emptyset_O = 1, \emptyset_R = 2, \emptyset_B = 1$)	0.901	0.765	0.707	0.669
Proposed method ($\emptyset_O = 2, \emptyset_R = 2, \emptyset_B = 1$)	0.884	0.743	0.688	0.663
Proposed method ($\emptyset_O = 3, \emptyset_R = 2, \emptyset_B = 1$)	**0.681**	**0.607**	**0.589**	**0.576**
Proposed method ($\emptyset_O = 2, \emptyset_R = 3, \emptyset_B = 1$)	0.711	0.647	0.603	0.582

TABLE 1. MAEs (m) among ROI-based algorithm and proposed method on object at sampling rates of 5%, 10%, 15%, and 20%

From TABLE 2 it can be seen that while MAEs of object area considerably decrease when applying proposed method by up to 43.83%, MAEs of object area slightly increase up to only 17.89%.

TABLE 3 and TABLE 4 presents a better performance of proposed method in MAEs of background and overall, which decreases up to 9.32%, 4.68%, respectively.

It should be noted that the MAE degradation mainly occurs on the road region; which is fairly low. Hence, the proposed sampling method provides an effective trade-off between errors on the object and those on the remaining areas.

	5%	10%	15%	20%
ROI-based sampling ($\alpha = 1, \beta = 1$)	0.208	0.159	0.132	0.123
ROI-based sampling ($\alpha = 4, \beta = 1$)	0.227	0.170	0.142	0.129
ROI-based sampling ($\alpha = 4, \beta = 0.25$)	0.419	0.267	0.220	0.180
Proposed method ($\emptyset_O = 1, \emptyset_R = 1, \emptyset_B = 1$)	0.249	0.174	0.147	0.134
Proposed method ($\emptyset_O = 2, \emptyset_R = 1, \emptyset_B = 1$)	0.274	0.186	0.157	0.141
Proposed method ($\emptyset_O = 1, \emptyset_R = 2, \emptyset_B = 1$)	0.183	0.155	0.136	0.118
Proposed method ($\emptyset_O = 2, \emptyset_R = 2, \emptyset_B = 1$)	0.247	0.173	0.146	0.132
Proposed method ($\emptyset_O = 3, \emptyset_R = 2, \emptyset_B = 1$)	0.267	0.182	0.151	0.136
Proposed method ($\emptyset_O = 2, \emptyset_R = 3, \emptyset_B = 1$)	**0.182**	**0.141**	**0.126**	**0.116**

TABLE 2. MAEs (m) among ROI-based algorithm and proposed method on road at sampling rates of 5%, 10%, 15%, and 20%

	5%	10%	15%	20%
ROI-based sampling ($\alpha = 1, \beta = 1$)	1.295	1.029	0.872	0.805
ROI-based sampling ($\alpha = 4, \beta = 1$)	1.450	1.102	0.948	0.902
ROI-based sampling ($\alpha = 4, \beta = 0.25$)	1.269	1.033	0.892	0.731
Proposed method ($\emptyset_O = 1, \emptyset_R = 1, \emptyset_B = 1$)	**1.186**	**0.881**	**0.758**	**0.692**
Proposed method ($\emptyset_O = 2, \emptyset_R = 1, \emptyset_B = 1$)	1.518	1.083	0.909	0.812
Proposed method ($\emptyset_O = 1, \emptyset_R = 2, \emptyset_B = 1$)	1.238	0.924	0.801	0.723
Proposed method ($\emptyset_O = 2, \emptyset_R = 2, \emptyset_B = 1$)	1.669	1.151	0.955	0.852
Proposed method ($\emptyset_O = 3, \emptyset_R = 2, \emptyset_B = 1$)	1.981	1.214	1.029	0.884
Proposed method ($\emptyset_O = 2, \emptyset_R = 3, \emptyset_B = 1$)	1.783	1.197	0.996	0.900

TABLE 3. MAEs (m) among ROI-based algorithm and proposed method on background at sampling rates of 5%, 10%, 15%, and 20%

	5%	10%	15%	20%
ROI-based sampling ($\alpha = 1, \beta = 1$)	0.793	0.647	0.551	0.513
ROI-based sampling ($\alpha = 4, \beta = 1$)	0.847	0.654	0.560	0.529
ROI-based sampling ($\alpha = 4, \beta = 0.25$)	0.853	0.660	0.579	0.521
Proposed method ($\emptyset_O = 1, \emptyset_R = 1, \emptyset_B = 1$)	**0.810**	**0.599**	**0.520**	**0.476**
Proposed method ($\emptyset_O = 2, \emptyset_R = 1, \emptyset_B = 1$)	0.848	0.626	0.538	0.491
Proposed method ($\emptyset_O = 1, \emptyset_R = 2, \emptyset_B = 1$)	0.832	0.619	0.541	0.489
Proposed method ($\emptyset_O = 2, \emptyset_R = 2, \emptyset_B = 1$)	0.929	0.651	0.556	0.505
Proposed method ($\emptyset_O = 3, \emptyset_R = 2, \emptyset_B = 1$)	0.981	0.672	0.572	0.516
Proposed method ($\emptyset_O = 2, \emptyset_R = 3, \emptyset_B = 1$)	0.954	0.673	0.571	0.516

TABLE 4. MAEs (m) among ROI-based algorithm and proposed method on overall at sampling rates of 5%, 10%, 15%, and 20%

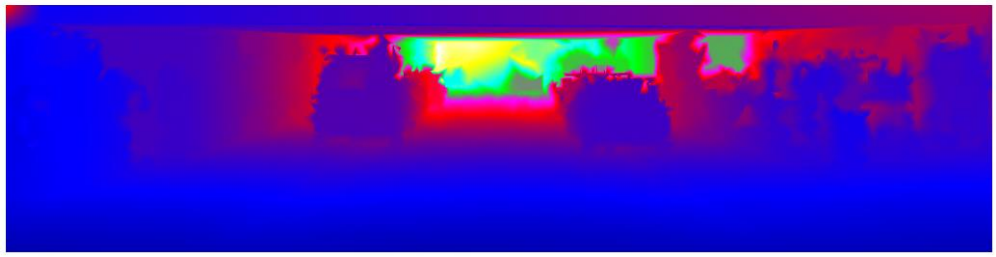

(a)

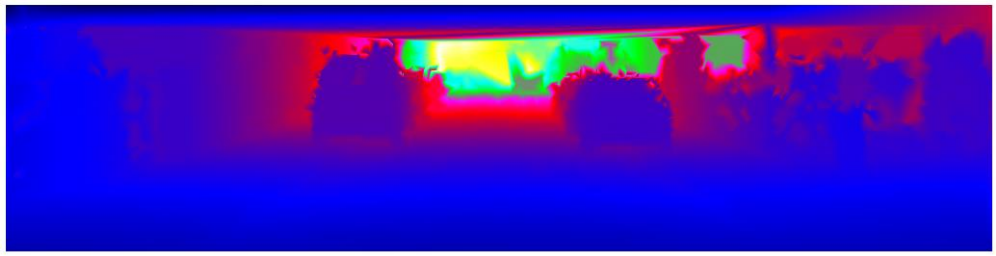

(b)

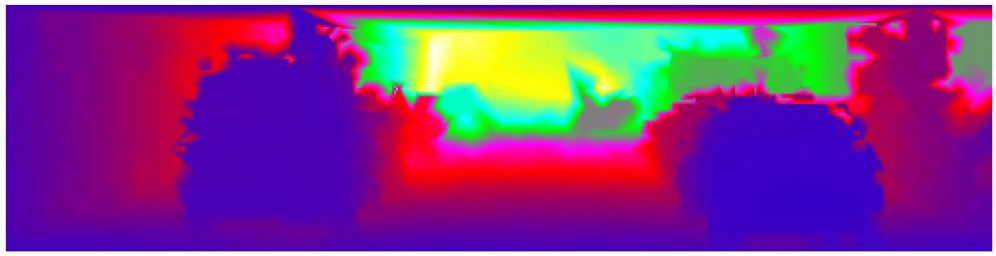

(c)

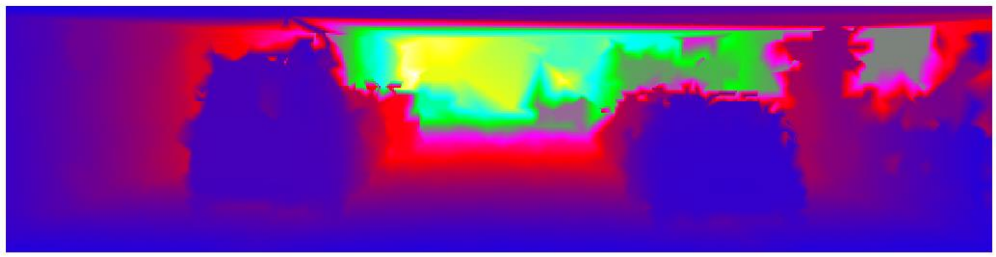

(d)

Figure 20. Reconstruction results at road and object regions by (a) ROI-Based Sampling algorithm, (b) Proposed method, and (c)-(d) the zoom-out results of object areas from (a)-(b), respectively.

Chapter 5. Conclusion

In this research, an optimized method of ROI-based LiDAR sampling algorithm in on-road environment for autonomous driving is proposed. With variations in the proposed method, they offer lower MAEs in object area and road areas and overall than the precedent research, and performs better than other sampling methods.

Appendix

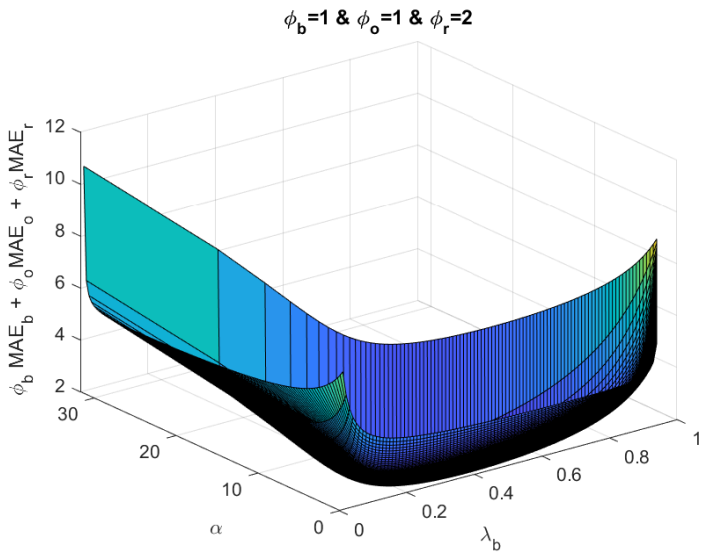

Figure 21. Graph of objective function

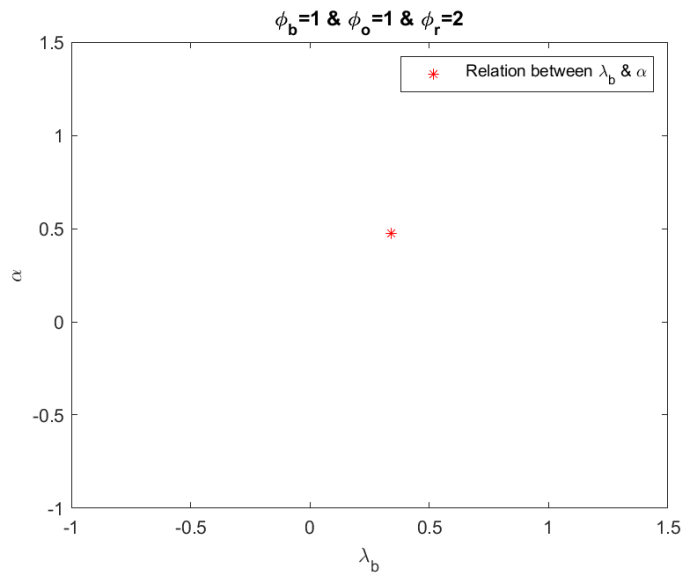

Figure 22. Relation between λ_b and α

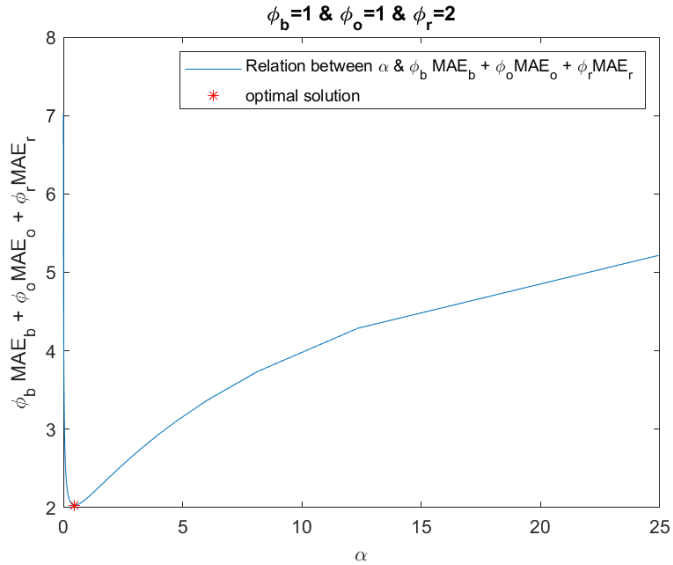

Figure 23. Relation between α and $\Phi_b MAE_b + \Phi_o MAE_o + \Phi_r MAEr$

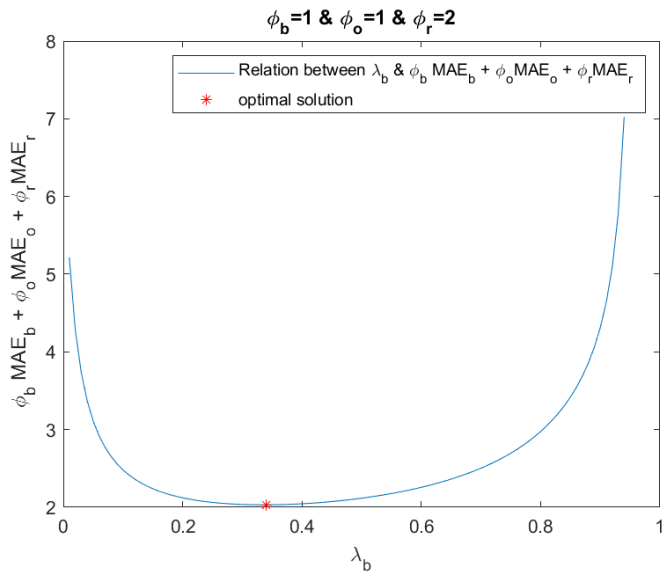

Figure 24. Relation between λ_b and $\Phi_b MAE_b + \Phi_o MAE_o + \Phi_r MAEr$

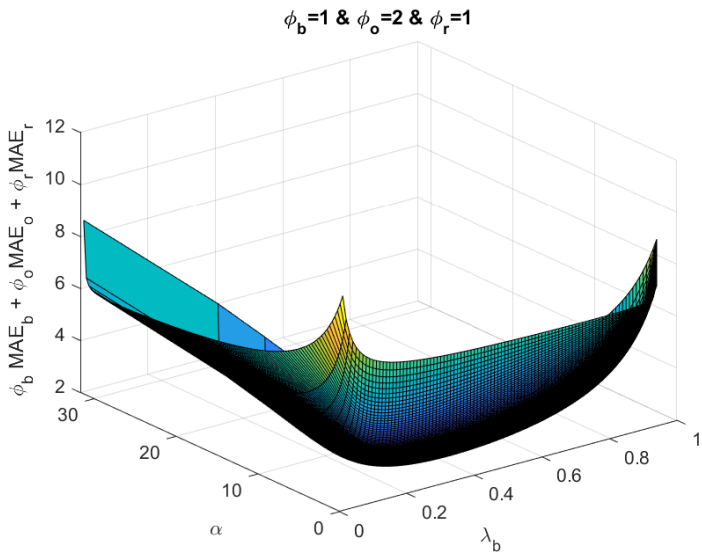

Figure 25. Graph of objective function

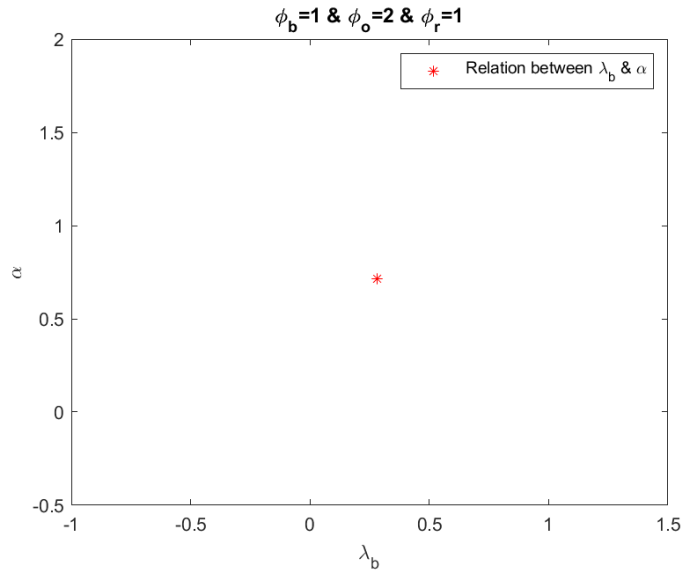

Figure 26. Relation between λ_b and α

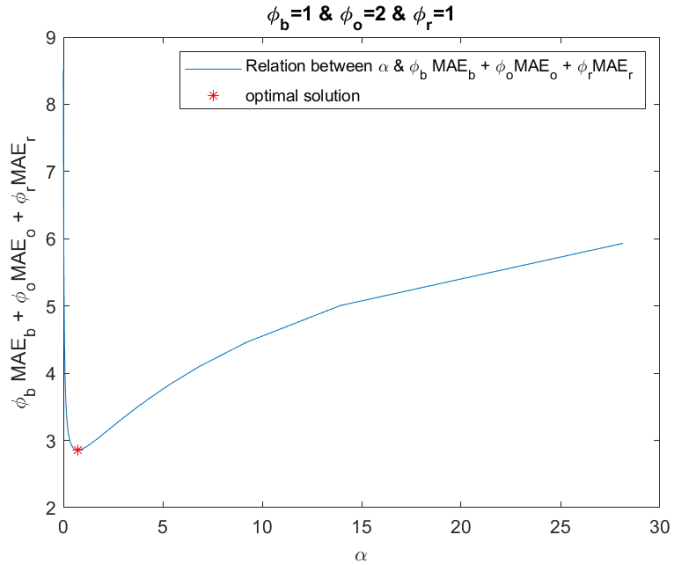

Figure 27. Relation between α and $\Phi_b MAE_b + \Phi_o MAE_o + \Phi_r MAEr$

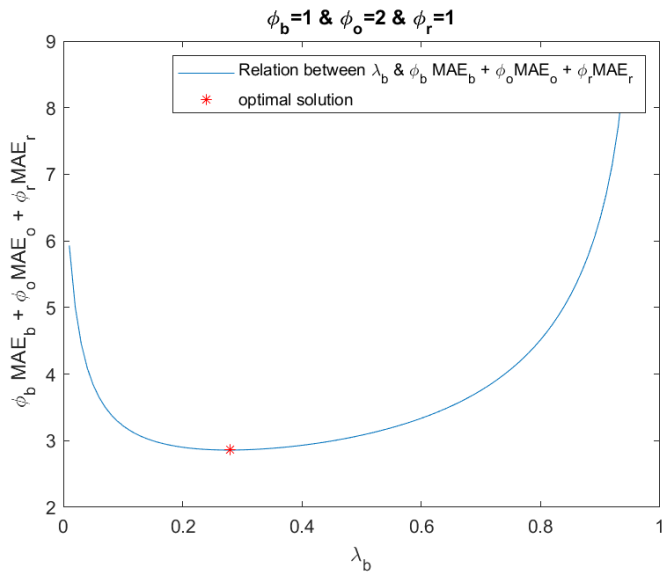

Figure 28. Relation between λ_b and $\Phi_b MAE_b + \Phi_o MAE_o + \Phi_r MAEr$

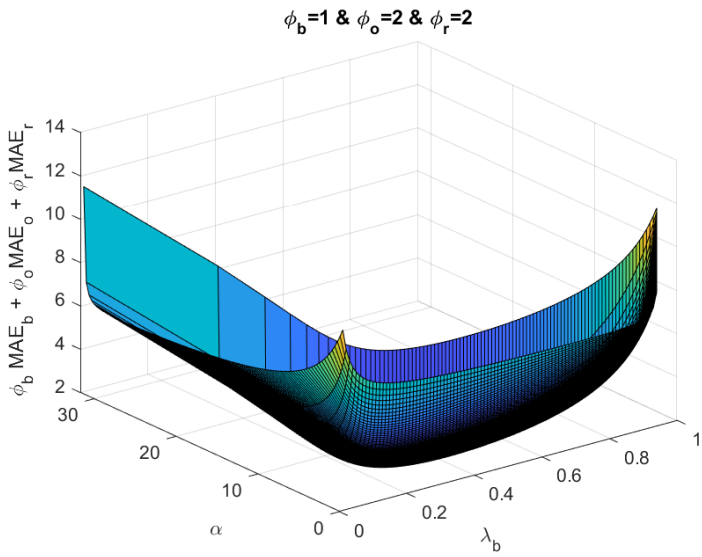

Figure 29. Graph of objective function

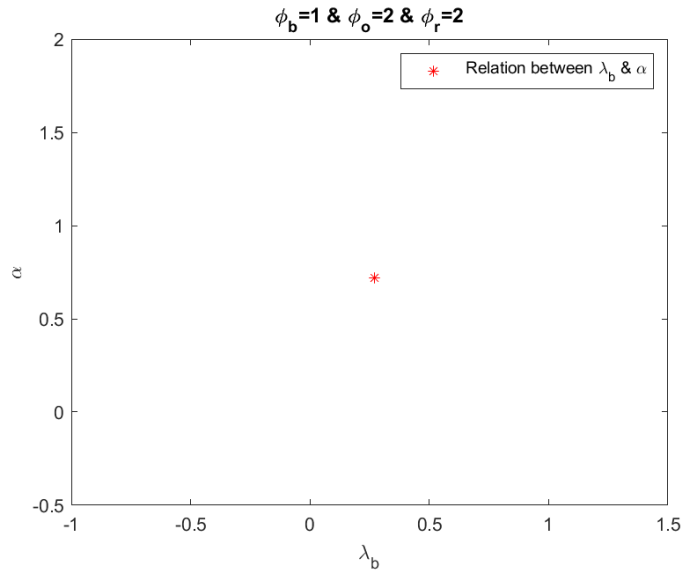

Figure 30. Relation between λ_b and α

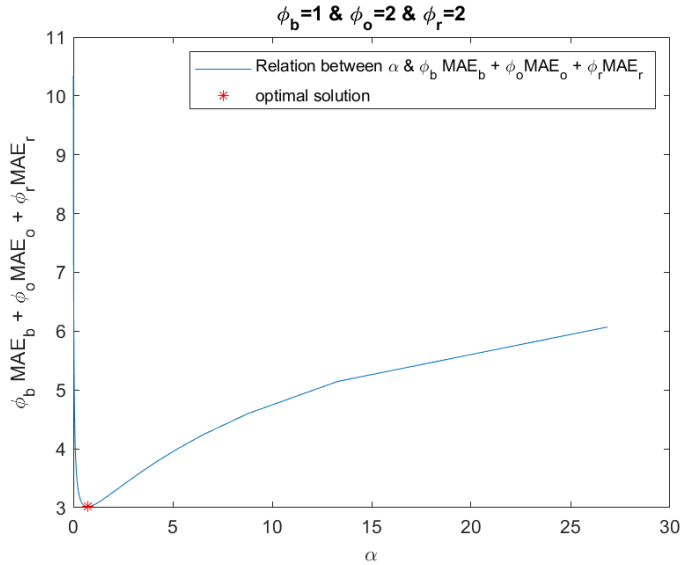

Figure 31. Relation between α and $\Phi_b MAE_b + \Phi_o MAE_o + \Phi_r MAEr$

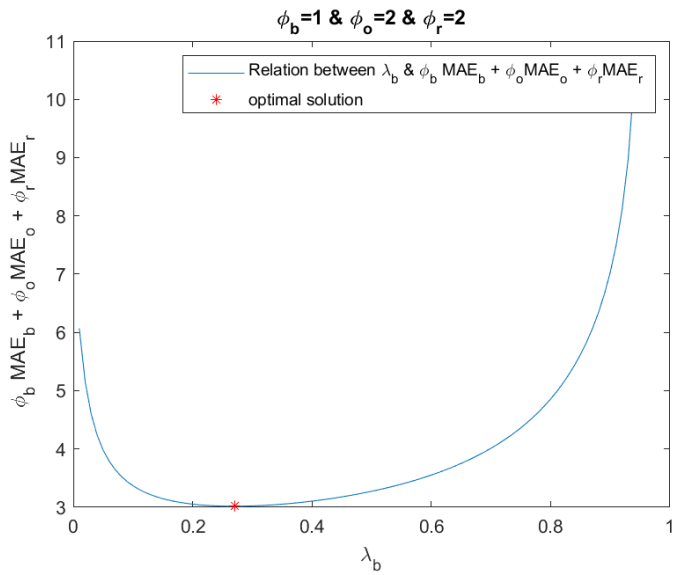

Figure 32. Relation between λ_b and $\Phi_b MAE_b + \Phi_o MAE_o + \Phi_r MAEr$

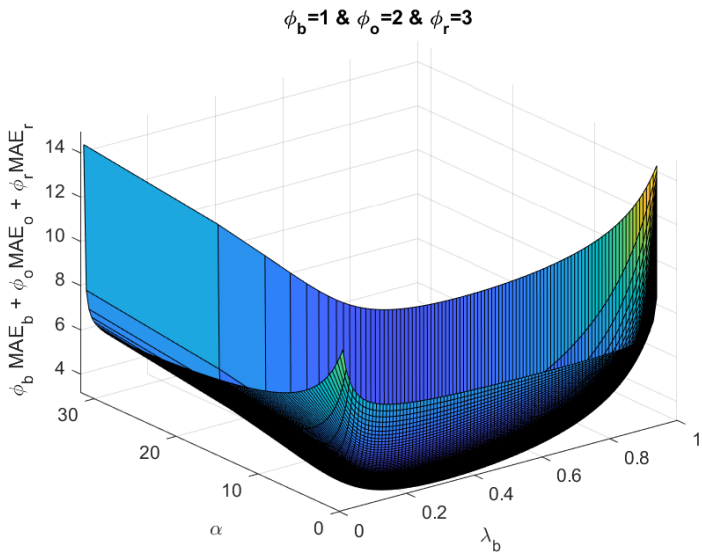

Figure 33. Graph of objective function

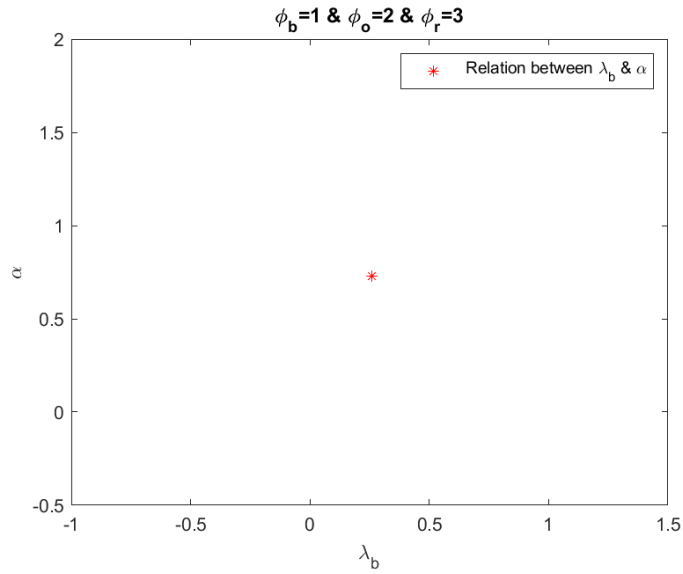

Figure 34. Relation between λ_b and α

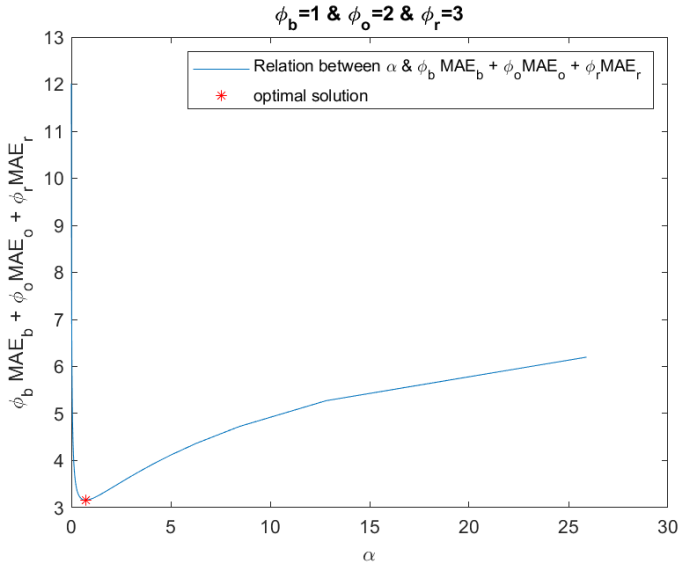

Figure 35. Relation between α and $\Phi_b MAE_b + \Phi_o MAE_o + \Phi_r MAEr$

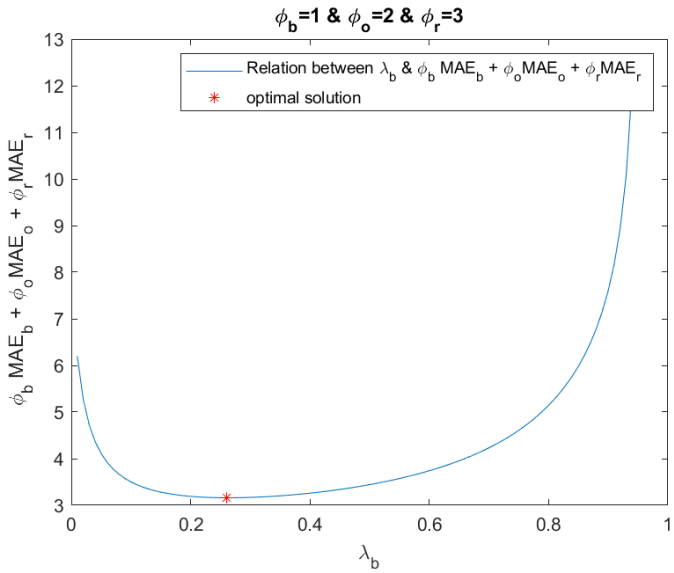

Figure 36. Relation between λ_b and $\Phi_b MAE_b + \Phi_o MAE_o + \Phi_r MAEr$

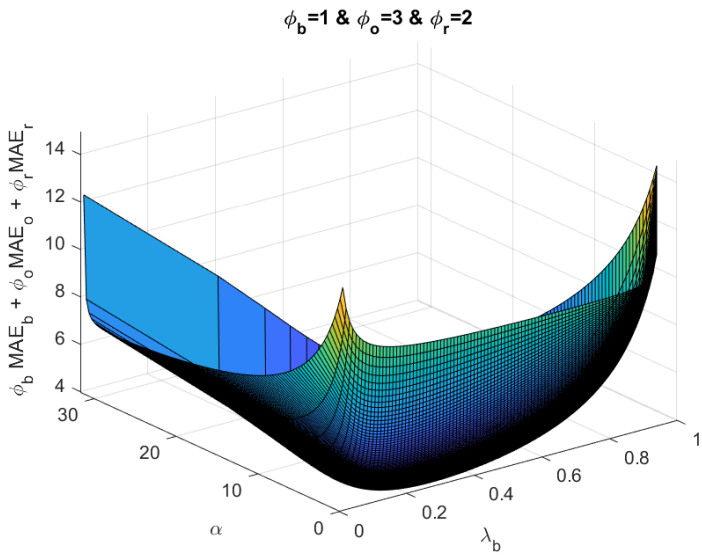

Figure 37. Graph of objective function

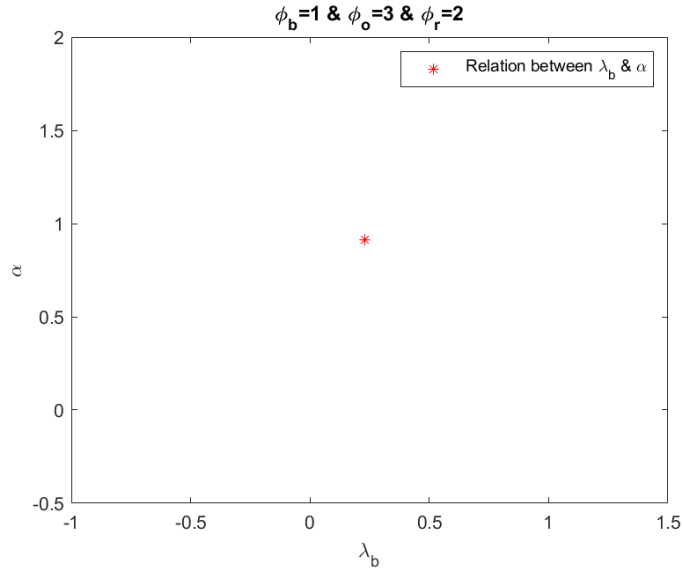

Figure 38. Relation between λ_b and α

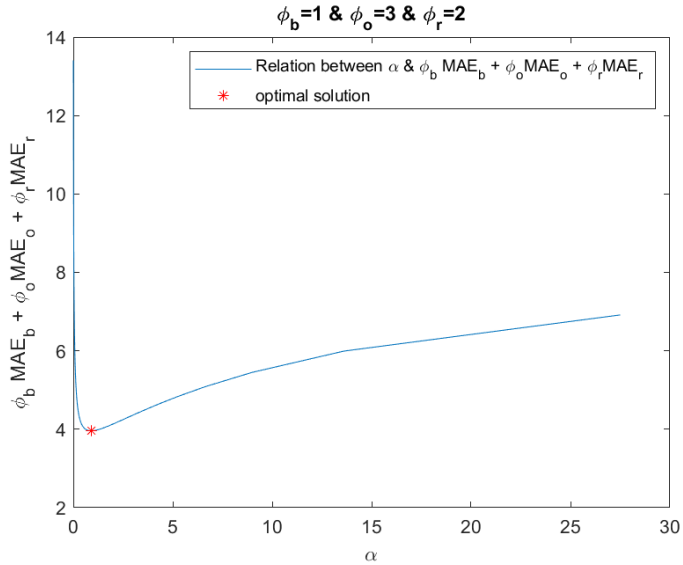

Figure 39. Relation between α and $\Phi_b MAE_b + \Phi_o MAE_o + \Phi_r MAEr$

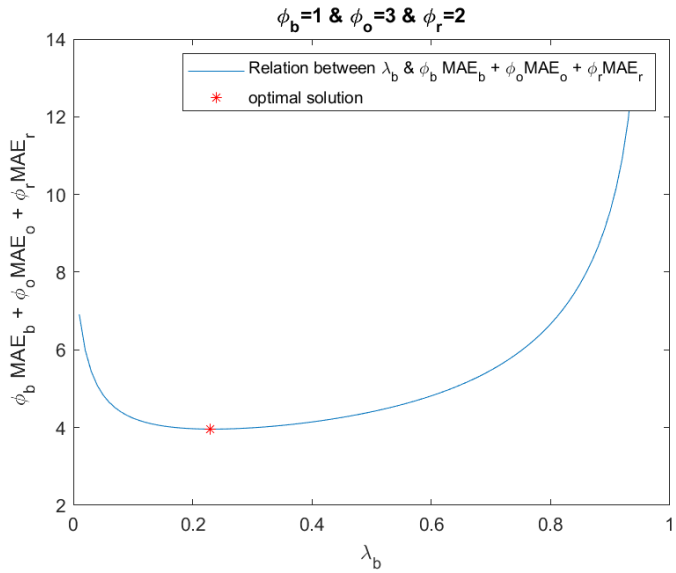

Figure 40. Relation between λ_b and $\Phi_b MAE_b + \Phi_o MAE_o + \Phi_r MAEr$

References

[1] "Driverless cars could lead to more traffic congestion," [Online]. Available: https://www.sciencedaily.com/releases/2019/10/191023104558.htm. [Accessed 18 May 2020].

[2] M. Maurer, C. J. Gerdes, B. Lenz and H. Winner, Autonomous Driving Technical, Legal and Socila Aspect, Spring Open.

[3] J. M. Anderson, N. Kalra, D. K. Stanley, C. Samaras and O. A. Oluwatola, "Autonomous Vehicle Implementation Predictions Implications for Transport Planning," Santa Monica CA: RAND, 2014.

[4] K. Bengler, K. Dietmayer, B. Färber, M. Maurer, C. Stiller and H. Winner, "Three decades of driver assistance systems," *IEEE Intelligent on Transportation Systems*, pp. 6-22, Winter 2014.

[5] P. L. C. S. a. R. U. A. Geiger, "Vision meets robotics: The," June 2012.

[6] P. a. R. A.Geiger, "Are we ready for Autonomous Driving? The KITTI Vision Benchmark Suite," 2012.

[7] Y.-G. H. a. S.-F. B.Prabhakaran, "Editorial IEEE transactions on multimedia special section on video analytics: Challenges, algorithms, and applications," *IEEE Transaction on Multimedia*, vol. 20, p. 1037, 2018.

[8] V. L. Inc., "Velodyne LiDAR HDL-64ES3: High Definition Real-Time 3D LiDAR Sensor.," 2017. [Online]. Available: http://velodynelidar.com/hdl-64e.html. [Accessed 18 May 2020].

[9] V. L. D. H.-J. L. a. H. K. X. T. Nguyen, "A high-definition LIDAR system based on two-mirror deflection scanners," *IEEE Sensors Journal* , vol. 18, p. 559‑568, 2018 .

[10] M. K. a. K. D. S. Hawe, "Dense disparity maps from sparse disparity measurements," 2011.

[11] A. W. a. D. A. C. S. Schwartz, "Multi-scale saliency-guided compressive sensing approach to efficient robotic laser range measurements," 2012.

[12] A. W. a. D. A. C. S. Schwartz, "Saliency-guided compressive sensing approach to efficient laser range measurement," *Journal of Visual Communication and Image Representation*, vol. 24, pp. 160-170, 2013.

[13] S. H. C. a. T. Q. N. L.-K. Liu, "Depth reconstruction from sparse samples: Representation, algorithm, and sampling," *IEEE Transaction on Image Processing* , vol. 24 , p. 1983‑1996, 2015.

[14] K.-T. N. H. K. a. H.-J. L. X.T. Nguyen, "ROI-based LiDAR Sampling Algorithm in On-road Environment for Autonomous Driving," *IEEE Access*, vol. 7, pp. 90243-90253, 2019.

초 록(Abstract in Korean)

Light detection and ranging (LiDAR) 센서는 최근 로보틱스와 자율 주행을 비롯한 여러 분야에서 사용되고 있다. 이런 LiDAR 센서는 다른 센서보다 낮은 해상도가 특징으로, 효과적인 샘플링 알고리즘을 설계하는 것이 필수적이다. 자율 주행에 적용되는 LiDAR 샘플링 알고리즘의 경우 도로의 복잡한 환경에서도 강인하게 높은 품질로 reconstruction을 하는 것이 목표이다. 이를 위해 현행 ROI 기반 샘플링 알고리즘은 시멘틱 정보를 이용하고 있다. 하지만, 객체, 도로, 배경 등에 따른 sampling rate는 지금까지 충분히 논의되지 않았고, 이로 인해 종합적인 reconstruction 품질이 저하될 수 있다. 이러한 문제를 해결하기 위해, 본 논문에서는 객체, 도로, 배경에 따른 sampling budget ratio를 도출할 수 있는 방법을 제안한다. 이 방법은 객체, 도로, 배경의 특성이 샘플링 이전에 선행 지식으로 주어져 있다는 가정을 이용한다. 제안하는 sampling budget을 적용한 결과, 현행 알고리즘보다 객체에 대한 mean-absolute-error (MAE)는 최대 45.92% 감소하였을 뿐만 아니라 전반적인 MAE 또한 3.36% 감소하였고, 도로에 대한 MAE는 오직 54.18% 감소하였다.

주요어: 샘플링 알고리즘, Light Detection and Ranging Sensor, LiDAR, 자율 주행, 도로 환경, ROI 기반 샘플링.
학번: 2018-27790